Semiconductor Electrodes

XLV. Photoelectrochemistry of n- and p-Type $MoTe_2$ in Aqueous Solutions

H. D. Abruña,* G. A. Hope, and A. J. Bard*

Department of Chemistry, University of Texas, Austin, Texas 78712

ABSTRACT

$MoTe_2$ (n- and p-type) electrodes have been characterized in terms of the energetic location of the valence and conduction bands, their voltammetric behavior, and their potential utility in photoelectrochemical cells. They show behavior that is qualitatively similar to the other layered semiconductors in terms of the sensitivity of their properties to growth conditions and surface imperfections. PEC cells based on n-$MoTe_2$ with I^-/I_2 as a redox couple were constructed. These reached monochromatic light (He/Ne laser) to electrical conversion efficiencies of over 8%.

Transition metal dichalcogenides have been used as electrodes in photoelectrochemical (PEC) cells that show good efficiency for the conversion of light to electrical energy and good stability (1). These materials, first described by Tributsch (2), have several advantages as electrodes: (*i*) the bandgaps (1.0-1.6 eV) are well matched with the solar spectrum; (*ii*) because the optical transition is d-d and involves nonbonding electrons, these semiconductors should be quite stable toward photodissolution; and (*iii*) they are composed of readily available nonprecious materials (W, Mo, S, Se, Te). Most studies of these materials have been with MoS_2, $MoSe_2$, and WSe_2. Another material in this series, $MoTe_2$, has some attractive properties (*e.g.*, bandgap $\simeq$ 1.0 eV) (3). However, only brief PEC studies of this material have been published (3). We report here the characterization of several n- and p-type $MoTe_2$ samples and their application in PEC cells.

Experimental

Crystal growth.—The α-$MoTe_2$ crystals were grown by halogen vapor transport from $MoTe_2$ powder (Great Western Inorganics, Golden, Colorado 99.9%). To transport crystals, a charge of 5g of $MoTe_2$ and the transport agent (for Br_2, 70 mg; $TeCl_4$, 100 mg) were introduced into a quartz tube (length, 19 cm; diameter, 18 mm), which was sealed after evacuation to a residual pressure of less than 5×10^{-5} Torr. Samples utilizing bromine transport were held at liquid nitrogen temperature during evacuation. The sealed tube with the powder distributed evenly along the length of the tube was introduced into a horizontal split tube furnace (Heavy-Duty Electric Company, Watertown, Wisconsin; 18 in. long, 1-1/4 in. diam) held at a maximum temperature of 875°C. The temperature decreased to approximately 800°C at the ends of the sample and increased crystal growth could be noted in these regions. The most favorable conditions for crystal growth, however, occurred where the tube was cooled by convection of air through the split in the furnace, with the majority of the crystals growing on the wall above the original charge.

Samples transported with bromine required 2-3 days to produce large crystals ($\sim$50 mm^2), whereas $TeCl_4$ could transport good crystals in approximately 18 hr. In both cases, an increased concentration of transport agent increased the growth rate; conditions for growth of the best crystals are those given above. Crystal growth occurred in clusters, away from the side of the tube, producing platelets of up to 1 cm^2 in area. Some crystals exhibited hexagonal growth spirals and many were twinned. However, a significant fraction had one flat crystal surface, and a few grew as flawless hexagonal plates from one corner. Electron microprobe analysis could not detect the presence of halogens in the transported crystals or any variation in composition between crystals. X-ray diffraction measurements confirmed the platelets to be semiconducting α-$MoTe_2$.

Electrodes.—Single crystals of $MoTe_2$ were selected from the clusters of crystals and cut with a razor blade to the desired dimensions. Back-ohmic contacts were made with Ga/In alloy (n-type) or with conductive silver paint (Acme Industries, New Haven, Connecticut) (p-type). Conductive silver paint was also used to secure a copper lead to the back of the crystals, which were then mounted in 6 mm bore glass tubing. The electrodes were masked with 5 min epoxy cement except for the surface to be illuminated (typically an area of 0.01-0.05 cm^2). The electrodes were illuminated with either an Oriel (Stamford, Connecticut) 450W Xe lamp (focused power $\sim$ 88 mW/cm^2) or a Spectra Physics 1.6 mW He/Ne laser. For long term irradiation, a commercial sunlamp ($\sim$60 mW/cm^2) was used in conjunction with a 12 cm water filter. Electrochemical instrumentation and techniques were as previously reported (4). A saturated sodium calomel reference electrode (SSCE) was employed. Capacitance measurements were performed as described earlier (1d). Aqueous solutions were made with triply distilled water. The o-phenylenediamine was recrystallized three times from CH_2Cl_2 and stored in the dark under N_2. All other reagents were of at least reagent grade quality and were used without further purification.

Results

Characterization of $MoTe_2$ electrodes.—As has been generally found with other layered semiconductors (5), the properties of $MoTe_2$ electrodes are strongly dependent on the condition of crystal growth as well as on the quality of the exposed surface. The results presented here are for selected crystals showing smooth surfaces ($\perp$C axis) free of exposed edges. The growth conditions had a pronounced effect on the properties exhibited by the electrodes; specimens that were n-type, p-type, compensated semiconductors, or showed metallic behavior were encountered. The best specimens obtained were of n-type grown by the $TeCl_4$ method described above, and most of the results presented here are concerned with these electrodes.

Capacitance measurements.—To determine the energetic location of the valence and conduction bandedges as well as the doping levels and flatband potentials, capacitance measurements were undertaken. A plot of capacitance *vs.* potential for a well-behaved n-type $MoTe_2$ electrode is shown in Fig. 1A. The specimen illustrated showed good behavior over a region of $\sim$1V with very little hysteresis. Well-behaved electrodes showed only minor frequency dispersion in the range of 100 Hz to 5 KHz. Other specimens, however, showed less ideal behavior, and in some instances severe hysteresis was noted. Capacitance data from well-behaved electrodes were used to construct Mott-Schottky (M-S) plots ($1/C^2$ *vs.* V). These gave good straight lines over a limited potential range (Fig. 1B); from the intercept a value of 0.19V *vs.* SSCE was estimated

* Electrochemical Society Active Member.

Key words: chalcogenides, layered semiconductors, photoelectrochemistry, solar energy conversion.

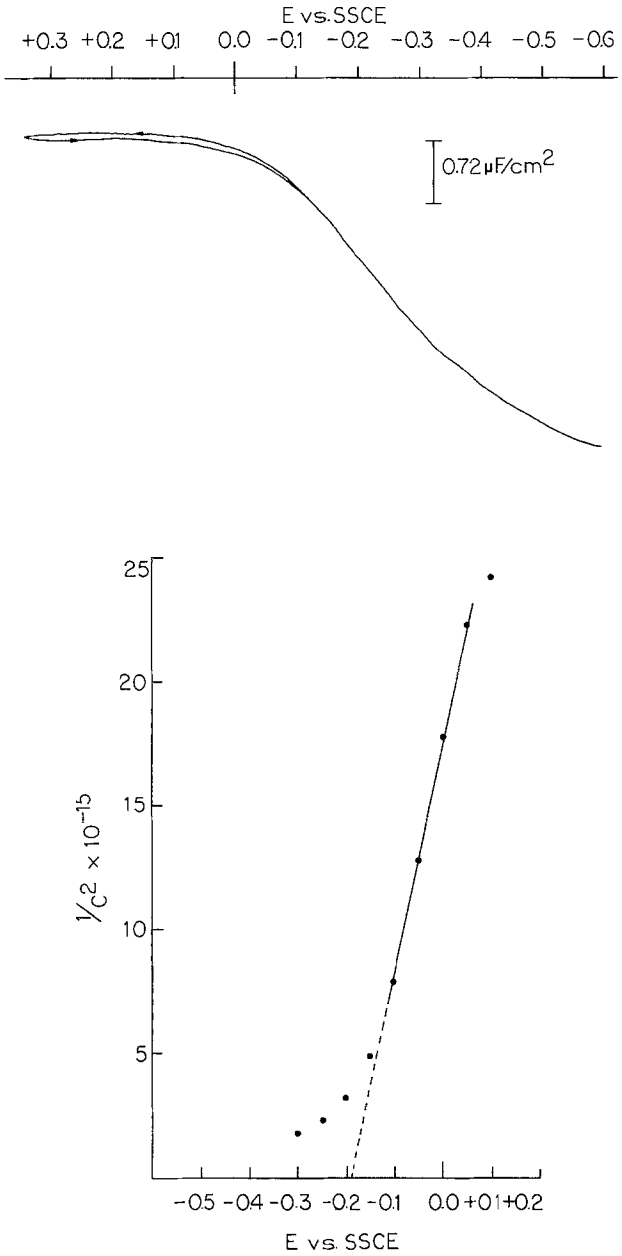

Fig. 1. (A, top) Capacitance-voltage curve for n-$MoTe_2$ in 0.5M aqueous Na_2SO_4 in the dark. Frequency 3 KHz; sweep rates 5 mV/sec[1]; a-c amplitude, 14 mV pp. (B, bottom) Mott-Schottky plot ($1/C^2$ vs. V) for n-$MoTe_2$ data from Fig. 1A.

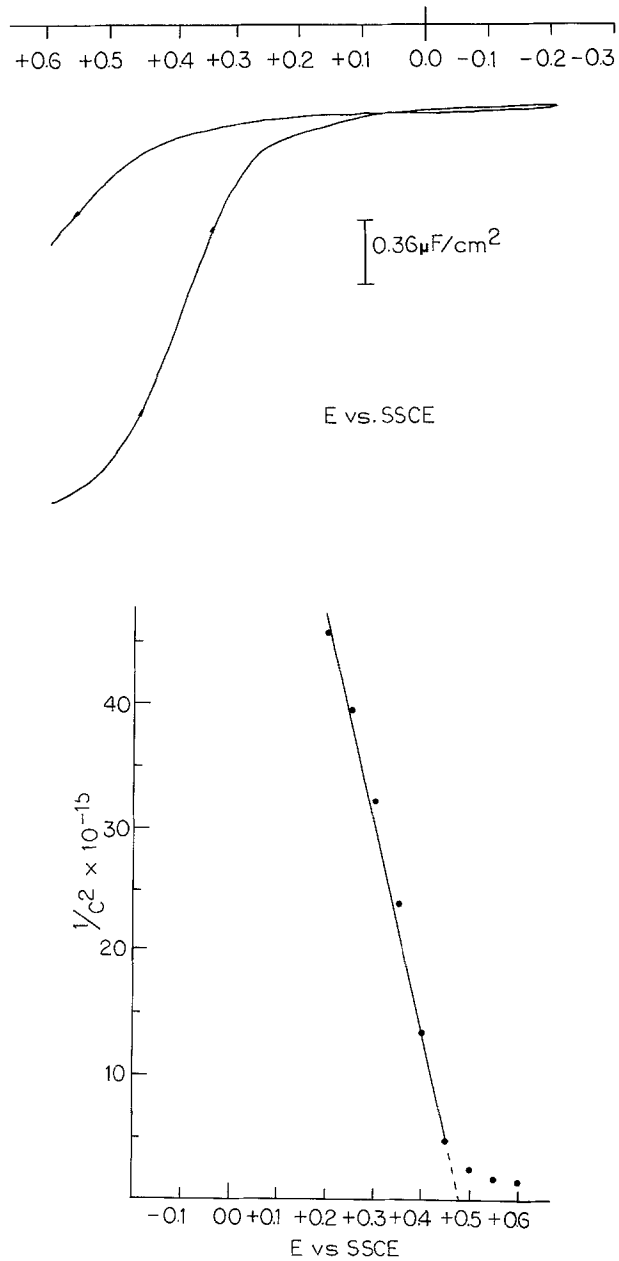

Fig. 2. (A, top) Capacitance-voltage curve for p-$MoTe_2$ in 0.5M aqueous Na_2SO_4 in the dark. Frequency 3 KHz; sweep rates 5 mV/sec[1]; a-c amplitude, 14 mV pp. (B, bottom) Mott-Schottky plot ($1/C^2$ vs. V) for p-$MoTe_2$ data from Fig. 2A.

for the flatband potential (V_{FB}). From the slope, a value for the donor density (N_D) of 1.8×10^{16} cm^{-3} was calculated. The crystals described above were used with either no further pretreatment or after peeling the top layer from the surface with adhesive tape. Electrodes that were treated for 30 sec with concentrated HCl showed essentially the same M-S plot behavior, except for a small decrease in the apparent donor densities (*i.e.*, they showed a steeper slope).

Capacitance-potential data for p-type electrodes were also obtained (Fig. 2A, B). Few measurements were made with these, however, because of the limited number of p-type specimens available. Rather severe hysteresis was observed in this case (Fig. 2A). However, if the data from the initial, negative going scan were used, linear M-S plots were obtained (Fig. 2B). From these, V_{FB} was estimated to be 0.48V *vs.* SSCE.

From the data presented above and the value of the bandgap energy, 1.0 eV, the positions of the valence and conduction bandedges for n- and p-type $MoTe_2$ electrodes could be estimated. The procedure is outlined below for n-type electrodes. The difference between E_C and E_F can be obtained from the equation

$$n_D = N_C \exp[-(E_C - E_F)/kT] \quad [1]$$

where n_D is the donor density (all donor impurities are assumed to be completely ionized); E_C is the energy at the edge of the conduction band, E_F, the Fermi level energy; and N_C, the density of effective states in the conduction band. This last term is given by

$$N_C = 2\left(\frac{2\pi M_e^* kT}{h^2}\right)^{3/2} \quad [2]$$

Taking the effective mass of the electron (M_e^*) as equal to that of the free electron (M_o) (which may introduce a significant error in calculating N_C), and assuming that the value for $MoTe_2$ is similar to that for $MoSe_2$ (6), we estimate N_C to be 2.6×10^{19} cm^{-3}. With this value and the experimental value for N_D, we find a difference of 0.18V between the Fermi level and the edge of the conduction band ($E_C - E_F$). This places the edge of the conduction band at -0.37V *vs.* SSCE. By subtracting the bandgap energy from this value, the location of the valence bandedge (E_V) is placed at $+0.63$V. A similar treatment of p-type electrodes places the valence and conduction bandedges at

+0.68 and −0.32V *vs.* SSCE, in good agreement with the results for n-type electrodes. These results suggest that couples with redox potentials (V_{redox}) within the gap, *i.e.*, positive of −0.4V and negative of 0.7V, should be appropriate for PEC cells with $MoTe_2$ electrodes.

Voltammetric behavior.—The voltammetric behavior in the dark and under illumination of n- and p-type $MoTe_2$ electrodes was investigated in aqueous solutions containing a variety of redox couples. For n-type electrodes, the I_3^-/I_2 and Fe(III/II) couples were used, whereas for p-type electrodes, $MV^{2+/+}$ (MV^{2+} is 4,4'-dimethylpyridinium or methylviologen) and the iron macrocycle [Fe(L)] (Fig. 3) used in a previous study (7) were employed. The voltammetric behavior of an n-type $MoTe_2$ electrode in contact with an I_3^-/I_2 solution in the dark and under illumination is shown in Fig. 4. In the dark (Fig. 4A), only very small anodic currents flow at potentials where I^- is oxidized readily at Pt because of the low concentration of minority carriers at the surface of the n-type semiconductor in the dark. Somewhat larger cathodic currents flow in the dark at about −0.2V *vs.* SSCE. These can be ascribed to the reduction of I_3^-, mediated perhaps by surface states. Under illumination, larger photoanodic currents flow (Fig. 4B); the photocurrent starts at about −0.2V *vs.* SSCE and saturates at ~ −0.05V. This represents an underpotential of ~0.5V for I^- oxidation. In addition, the voltammetric behavior under chopped illumination shows that recombination effects are minor.

With the $Fe^{3+/2+}$ electrolyte, the behavior is rather poor. Here, the electrodes exhibited small photoanodic currents (<50 $\mu A/cm^2$), small underpotentials (~150 mV), and substantial recombination effects. The voltammetric behavior of p-type electrodes in the presence of MV^{2+} and Fe(L) is shown in Fig. 5 and 6, respectively. The cathodic dark currents were very low (Fig. 5A) because of the small density of minority carriers (electrons) at the electron surface. Upon illumination in the presence of MV^{2+}, photocathodic currents flow. These have an onset at −0.2V and saturate at −0.35V (Fig. 5B). However, substantial backanodic current also flows. The voltammetric behavior under chopped illumination indicates that recombination is rather severe in this case. This behavior has also been observed for p-WSe_2 electrodes in methylviologen solutions (8). These recombination effects are largely eliminated by the use of the iron macrocycle described previously (7). However, the photocurrents are very small (Fig. 6).

Photoelectrochemical cells.—To assess the potential utility of $MoTe_2$ electrodes for solar energy conversion, several two-electrode PEC cells were constructed. Since the best voltammetric results were obtained on n-type electrodes and since the number of p-type specimens was very limited, only n-type electrodes were studied. In all cases, the cells were constructed by connecting the semiconductor electrode to a large

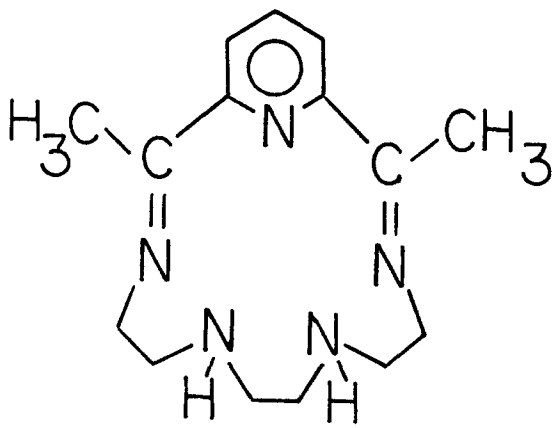

Fig. 3. Structure of macrocyclic ligand, L

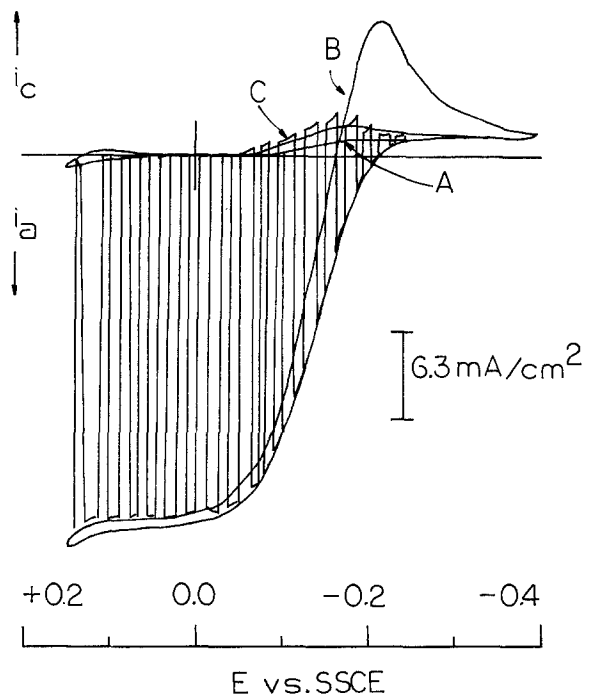

Fig. 4. Voltammetric behavior of n-$MoTe_2$ in aqueous 5M I^-, 10 mM I_2; sweep rate, 20 mV/sec (A) in the dark; (B) under illumination with an He/Ne laser, power ~ 80 mW/cm^2; (C) under chopped illumination (sweep rate, 10 mV/sec).

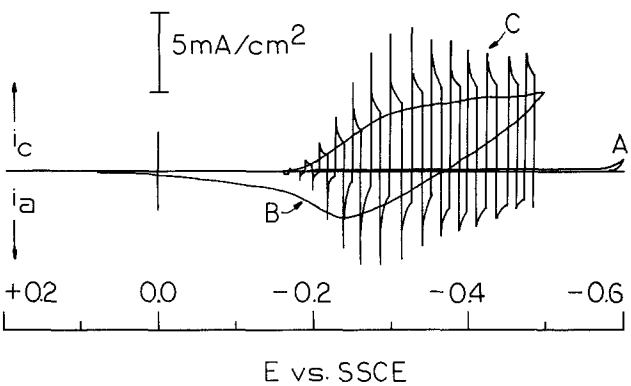

Fig. 5. Voltammetric behavior of p-$MoTe_2$ in aqueous 0.7M KCl, 0.2M MV^{2+}; sweep rate, 20 mV/sec (A) in the dark; (B) under illumination with an He/Ne laser, power ~ 80 mW/cm^2; (C) under chopped illumination (sweep rate, 10 mV/sec).

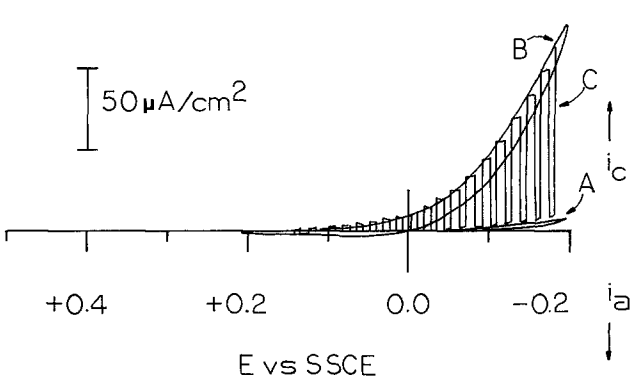

Fig. 6. Voltammetric behavior of p-$MoTe_2$ in aqueous 0.5M Na_2SO_4, 0.3M $Fe(L)^{3+}$; sweep rate, 20 mV/sec (A) in the dark; (B) under illumination with an He/Ne laser, power ~ 80 mW/cm^2; (C) under chopped illumination (sweep rate, 10 mV/sec).

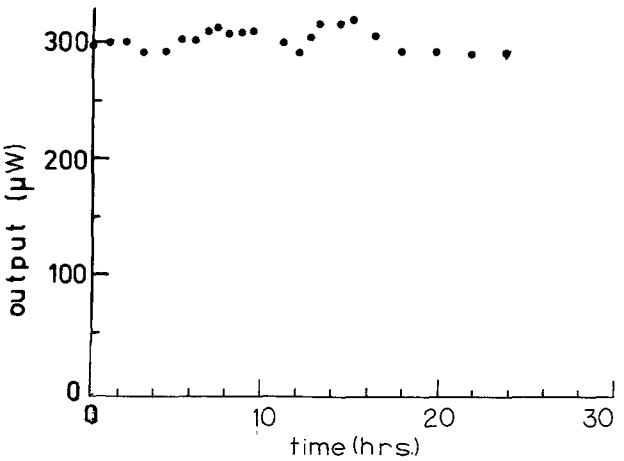

Fig. 7. Power curve (photocurrent vs. photovoltage) for PEC cell n-$MoTe_2$/aqueous 5M I^-, 10 mM I_2/Pt under illumination with an He/Ne laser, power input = 80 mW/cm^2.

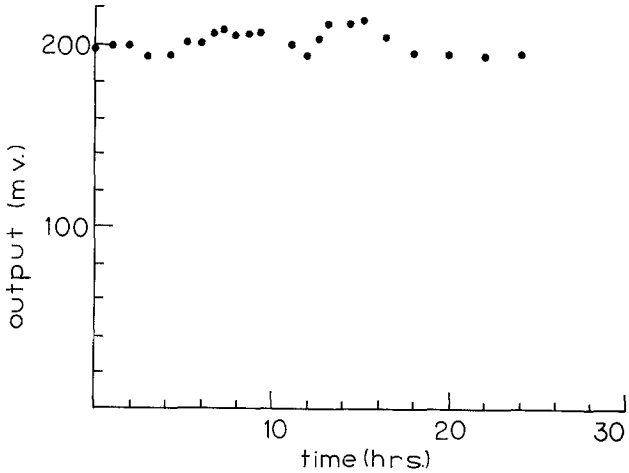

Fig. 8. Plot of output (near maximum power point) vs. time for an n-$MoTe_2$ electrode in contact with an aqueous 5M I^-, 10 mM I_2 solution. Input power from a commercial sunlamp ~ 60 mW/cm^2.

area Pt electrode through an external load. The redox couple used was I^- (5*M*), I_2 (10 m*M*). The results obtained with several specimens are given in Table I and the power characteristics for one such cell are shown in Fig. 7. As can be seen from the data in Table I, different electrodes give cells with widely different efficiencies and fill factors. This probably reflects differences in growth conditions and surface imperfections. However, a monochromatic efficiency of 8% was found with one cell under red (He/Ne laser) illumination. Furthermore, the output of these cells was quite stable with time with no decay (±10%) noticed during 20 hr of operation near the maximum power point (Fig. 8).

Surface treatments.—We previously reported (9) the improvement of performance of PEC cells based on n-$MoSe_2$ and n-WSe_2 electrodes after the dark electropolymerization of o-phenylenediamine, which was thought to block recombination centers (edges) on the electrode surface. This procedure was also investigated with $MoTe_2$. The polymerization generally had beneficial effects with improvements of 10-15% obtained (Fig. 9). The somewhat lower relative improvement in performance obtained for n-$MoTe_2$ relative to n-$MoSe_2$ and n-WSe_2 can probably be attributed to the relatively defect-free surfaces of the $MoTe_2$ crystals.

Conclusions

$MoTe_2$ electrodes have been characterized in terms of the energetic location of the valence and conduction bands, their voltammetric behavior, and their potential utility in PEC cells. Qualitatively they show behavior similar to the other layered compounds in terms of the sensitivity of their behavior to growth conditions and surface imperfections. Although the monochromatic (red-light) energy conversion efficiencies achieved (8%) are lower than those for other layered compounds, they could be of potential use if incorporated into polycrystalline layers. The location of the valence and conduction band edges is such that a wide choice of redox couples could in principle be used.

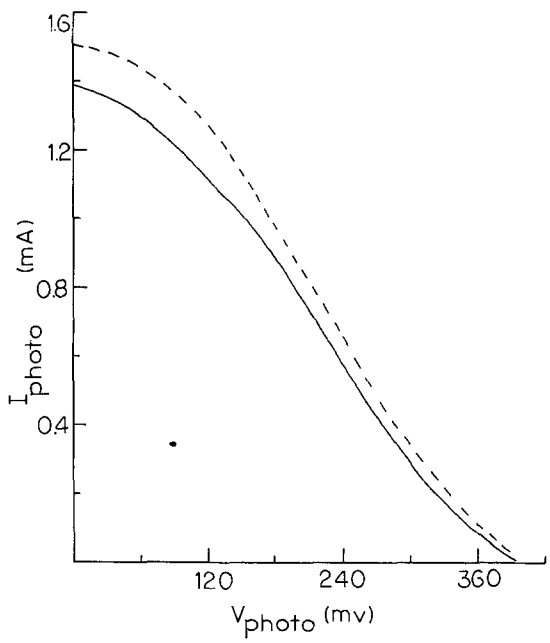

Fig. 9. Power curves for an n-$MoTe_2$ electrode in contact with an aqueous 5M I^-, 10 mM I_2 solution under illumination with an He/Na laser, power input ~ 80 mW/cm^2 before (solid curve) and after (dashed curve) dark polymerization of o-phenylenediamine.

Table I. Characteristics for photoelectrochemical cells based on n-$MoTe_2$[a]

i_{ss}[b] (mA/cm^2)	V_{oc}[c] (mV)	ff[d]	η%[e]
30	350	0.40	5.1
14	381	0.26	1.3
16	408	0.32	2.6
38	378	0.28	5.0
18	360	0.33	2.6
26	338	0.38	4.2
34	373	0.51	8.1

[a] Aqueous I- (5*M*), I_2 (0.01*M*); input power from an He/Ne laser, ~80 mW/cm^2.
[b] Short-circuit photocurrent.
[c] Open-circuit photovoltage.
[d] Fill factor.
[e] Light to electrical power conversion efficiency.

Acknowledgment

The support of this research by the National Science Foundation (CHE 8000682) and the Solar Energy Research Institute is gratefully acknowledged. G. A. Hope is on leave from Griffith University, Nathan, QLD, Australia.

Manuscript submitted Dec. 28, 1981; revised manuscript received *ca.* April 8, 1982.

Any discussion of this paper will appear in a Discussion Section to be published in the June 1983 JOURNAL. All discussions for the June 1983 Discussion Section should be submitted by Feb. 1, 1983.

Publication costs of this article were assisted by the University of Texas.

REFERENCES

1. (a) For a general overview of these materials, see J. A. Wilson and A. D. Yoffe, *Adv. Phys.*, **18**, 193 (1969); (b) F. R. Fan, H. S. White, B. Wheeler, and A. J. Bard, *This Journal*, **127**, 518 (1980); (c) D. Canfield and B. A. Parkinson, *J. Am. Chem. Soc.*, **103**, 1279 (1981); (d) H. S. Lewerenz, A. Heller, and T. J. DiSalvo, *ibid.*, **102**, 1877 (1980); (e) F. R. Fan and A. J. Bard, *This Journal*, **128**, 945 (1981); (f) L. F. Scheenmeyer and M. S. Wrighton, *J. Am. Chem. Soc.*, **101**, 6496 (1979); (g) H. Tributsch, *Disc. Faraday Soc.*, **70**, 189 (1980).
2. (a) H. Tributsch and J. S. Bennett, *J. Electroanal. Chem. Interfacial Electrochem.*, **81**, 97 (1971); (b) H. Tributsch, *This Journal*, **125**, 1086 (1978); (c) H. Tributsch, *Ber. Bunsenges. Phys., Chem.*, **81**, 361 (1977); (d) H. Tributsch, *ibid.*, **82**, 69 (1978).
3. H. Tributsch, H. Gerischer, C. Clemen, and E. Bucher, *Ber. Bunsenges. Phys. Chem.*, **83**, 655 (1979).
4. H. D. Abruña and A. J. Bard, *J. Am. Chem. Soc.*, **103**, 6898 (1981).
5. (a) S. Ahmed and H. Gerischer, *Electrochim. Acta*, **24**, 705 (1979); (b) H. S. White, F. R. Fan, and A. J. Bard, *J. Electroanal. Chem. Interfacial Electrochem.*, **128**, 1045 (1981); (c) W. Kautek, H. Gerischer, and H. Tributsch, *Ber. Bunsenges. Phys. Chem.*, **83**, 1000 (1980); (d) W. Kautek and H. Gerischer, *ibid.*, **84**, 645 (1980).
6. W. T. Hicks, *This Journal*, **111**, 1058 (1964).
7. H. D. Abruña and A. J. Bard, *ibid.*, **129**, 673 (1982).
8. H. S. White, Unpublished results.
9. H. S. White, H. D. Abruña, and A. J. Bard, *This Journal*, **129**, 265 (1982).

Solubility of Yttrium Oxide in Na_2SO_4 and NaCl Melts

M.L. Deanhardt,*[1] and Kurt H. Stern*

Chemistry Division, Naval Research Laboratory, Washington, D.C. 20375

ABSTRACT

Equilibrium constants for the acidic and basic dissolution reactions of Y_2O_3, $Y_2O_3 = 2Y^{+3} + 3O^{2-}$, and $Y_2O_3 + O^{2-} = 2YO_2^-$, respectively, have been measured in molten NaCl at 1100 K and in molten Na_2SO_4 at 1200 K by coulometric and potentiometric titrations. In NaCl, the equilibrium constants on an ion fraction scale are $(1.4\text{-}2.2) \times 10^{-36}$ and $(0.7\text{-}5.5) \times 10^{-3}$, respectively; in Na_2SO_4, the constants are $(4.5\text{-}6.4) \times 10^{-31}$ and $(0.1\text{-}1.4) \times 10^{-2}$.

Extensive corrosion of metals occurs in gas turbines that operate in marine or other salt-contaminated environments (1). Corrosion is accelerated when a thin film of molten salt (mainly Na_2SO_4) covers the metal surface. The molten salt comes directly from ingested salts and/or from the reaction of sodium chloride with O_2 and sulfur in fuels, which forms Na_2SO_4 (2).

Metals or alloys which are subjected to this type of high temperature corrosion are normally protected by surface oxide scales such as Cr_2O_3 or Al_2O_3. The overall oxidation resistance of these scales can be improved by addition of reactive elements such as yttrium, silicon, titanium, zirconium, and hafnium (3). Some beneficial effects of these additions are enhancement of the scale adherence, reduction of the scale growth rate, enhancement in the selective oxidation of the protective scale-forming element, and suppression of void formation at the alloy-scale interface (4).

One of the factors that affects the oxidation resistance of the protective scales is the solubility of the metal oxides in molten Na_2SO_4. Recently, the solubilities of several important metal oxides, such as Cr_2O_3 (5), Al_2O_3 (5), Co_3O_4 (6, 7), and NiO (6, 7), were measured in molten Na_2SO_4. The purpose of this work is to report the solubility of yttria, (Y_2O_3), in both molten Na_2SO_4 and NaCl. The solubility of Y_2O_3 was determined by coulometric titration of YCl_3 (in molten NaCl) and $Y_2(SO_4)_3$ (in molten Na_2SO_4) with electrochemically generated oxide ions, using a stabilized zirconia (SZ) electrode as an oxide ion source. Data from the titration curves allow one to calculate metal oxide solubility as a function of salt basicity. We expect that data of this sort will advance the understanding of metal-salt reactions at high temperatures.

Experimental

All coulometric titrations, weighings, and material handling were carried out in a glove box (Vacuum Atmospheres) containing an O_2/He atmosphere in which H_2O and CO_2 were kept at the 1-10 ppm level. The oxygen pressure over the melts was measured with a Beckman Model E2 oxygen analyzer and was kept near 20%. Measurements in molten NaCl were carried out at 1100 ± 5 K and in molten Na_2SO_4 at 1200 ± 5 K.

Materials.—Reagent grade NaCl and Na_2SO_4 (Fisher Scientific) were vacuum-dried at 500°C before use. Anhydrous YCl_3 was prepared from $YCl_3 \cdot 6H_2O$ (Alfa Products). The $YCl_3 \cdot 6H_2O$ was heated to 750°C (melting point, 709°C) under flowing HCl for 24 hr, cooled, and purged with argon. The resulting YCl_3 was calculated from the weight change to be 99.4% pure. Anhydrous $Y_2(SO_4)_3$ (99.9%), anhydrous Y_2O_3 (99.99%), and reagent Na_2O (all from Alfa Products) were used without pretreatment. The reagent Na_2O was found to contain 94% Na_2O by analysis with ~2% Na_2O_2 impurity.

High purity (99.8%) alumina crucibles were used as melt containers in the coulometric titrations. Glazed porcelain boats were used as melt containers in the preparation of samples for x-ray analysis.

Coulometric titrations.—These titrations were carried out with two electrode pairs: one pair, consisting of a stabilized zirconia and Ag reference electrode, measures the Na_2O activity in the melt; while the other pair, consisting of an O^{2-} conducting zirconia electrode and an Na^+-ion conducting counterelectrode, titrates O^{2-} ions into the melt. The experimental arrangement and equations have previously been described in detail (7, 8) for the solubility measurements of nickel and cobalt oxides in molten NaCl and Na_2SO_4. In the present work, dilute solutions of YCl_3 in NaCl and $Y_2(SO_4)_3$ in Na_2SO_4 were titrated with coulometrically generated O^{2-}.

Potentiometric titrations.—To aid in the interpretation of the coulometric titration curves and to determine the oxide precipitation and dissolution reactions (see below), potentiometric titrations of Y^{+3}-contain-

* Electrochemical Society Active Member.
[1] Present address: Chemistry Department, George Mason University, Fairfax, Virginia 22030.
Key words: ceramics, coulometry, potentiometry, yttria.